Polycrystalline Well-Shaped Blocks of Indium Oxide Obtained by the Sol−Gel Method and Their Gas-Sensing Properties

Alexander Gurlo,*,† Nicolae Barsan,† Udo Weimar,† Maria Ivanovskaya,‡ Antonietta Taurino,§ and Pietro Siciliano§

Institute of Physical and Theoretical Chemistry, University of Tübingen, Auf der Morgenstelle 8, 72076 Tübingen, Germany, Scientific Research Institute for Physical and Chemical Problems, Belarus State University, Leningradskaya 14, 220050 Minsk, Belarus, and Istituto per la Microelettronica e i Microsistemi, IMM-CNR, Sezione di Lecce, Via Arnesano, 73100 Lecce, Italy

Received August 6, 2003

Aging-induced aggregation of the nanoparticles in the colloidal solution of indium hydroxide leads to the formation of micrometer particles in the form of well-shaped blocks. As shown by high-resolution transmission electron microscopy and selected area electron diffraction, the well-shaped blocks have a polycrystalline nature composed of small nanounits. After calcination at 400 °C, they consist of cubic and hexagonal In_2O_3. Semiconducting sensors, composed of well-shaped blocks of cubic and hexagonal In_2O_3, show high sensitivity to low levels of ozone in the air.

Introduction

Indium oxide (In_2O_3)—an n-type semiconductor (band gap 3.5−3.7 eV)—is of interest for many device applications and fundamental research. As In_2O_3 films exhibit good electrical conductivity and high transparency in the visible region, they find many technological applications in electronic devices of various types, that is, photovoltaic devices, liquid-crystal displays, and solar cells.[1−3] The sol−gel-prepared In_2O_3 films and powders are of interest for gas-sensing applications, for example, detection of low concentrations of oxidizing gases, such as NO_2 and O_3.[4−6] There are several works which showed that thin and thick films based on cubic In_2O_3 are very sensitive to low concentrations (below 100 ppb) of NO_2 and O_3 in the air and almost insensitive to CO.[5−8] Many properties of sol−gel-obtained films and powders, among them gas sensitivity, strongly depend on the crystal structure, grain size, and history of the In_2O_3. It was shown that the best results in terms of NO_2 response correspond to sol−gel-prepared In_2O_3 films with the average grain size between 5 and 30 nm.[5] Therefore, the preparation of In_2O_3 particles with controlled crystal structure and grain size and shape are of great importance for practical applications.

In recent years sub- and micrometer In_2O_3 particles uniform in size and shape have been produced by soft-chemical methods, for example, by sol−gel method,[9,10] by controlled precipitation in homogeneous solution,[11] by double-jet precipitation,[12] by forced hydrolysis,[13] and by sonohydrolysis.[14] All these methods allow one to obtain sub-micrometer indium hydroxide particles with different shapes and morphologies, from spherical to rodlike ones. The original shape of the particles is kept even after the calcinations and the phase transformation of $In(OH)_3$ into In_2O_3, which occurs in the air at 200−260 °C. In some works it was speculated that the micrometer particles of $In(OH)_3$ are probably composed of the smaller nanosized subunits[10,13,14] and therefore they have a polycrystalline nature. But the authors did not give any evidence for that and therefore this supposition was not proved. In our previous study[15] we have already observed the formation of such micrometer

* Corresponding author. E-mail: alexander.gurlo@ipc.uni-tuebingen.de. Phone: +49-7071-2978765. Fax: +49-7071-295960. http://www.ipc.uni-tuebingen.de.
† University of Tübingen.
‡ Belarus State University.
§ IMM-CNR.

(1) Evans, K. A. In *Chemistry of aluminium, gallium, indium and tallium*; Downs, A. J., Ed.; Chapman & Hall: London, 1993.
(2) Murali, A.; Barve, A.; Leppert, V. J.; Risbud, S. H.; Kennedy, I. M.; Lee, H. W. *Nano Lett.* **2001**, *1*, 287−289.
(3) Poznyak, S. K.; Talapin, D. V.; Kulak, A. I. *J. Phys. Chem. B* **2001**, *105*, 4816−4823.
(4) Gurlo, A.; Ivanovskaya, M.; Pfau, A.; Weimar, U.; Göpel, W. *Thin Solid Films* **1997**, *307*, 288−293.
(5) Gurlo, A.; Barsan, N.; Ivanovskaya, M.; Weimar, U.; Göpel, W. *Sens. Actuators B* **1998**, *47*, 92−99.
(6) Atashbar, M. Z.; Gong, B.; Sun, H. T.; Wlodarski, W.; Lamb, R. *Thin Solid Films* **1999**, *354*, 222−226.
(7) Starke, T. K. H.; Coles, G. S. V.; Ferkel, H. *Sens. Actuators B* **2002**, *85*, 239−245.
(8) Steffes, H.; Imawan, C.; Solzbacher, F.; Obermeier, E. *Sens. Actuators B* **2001**, *78*, 106−112.
(9) Tahar, R. B. H.; Ban, T.; Ohya, Y.; Takahashi, Y. *J. Appl. Phys.* **1997**, *82*, 865−869.
(10) Perez-Maquela, L. A.; Wang, L.; Matijevic, E. *Langmuir* **1998**, *14*, 4397−4401.
(11) Yura, K.; Fredrikson, K. C.; Matijevic, E. *Colloids Surf.* **1990**, *50*, 281−286.
(12) Wang, L.; Perez-Maqueda, L. A.; Matijevic, E. *Colloid Polym. Sci.* **1998**, *276*, 847−850.
(13) Hamada, S.; Kudo, Y.; Kobayashi, T. *Colloids Surf. A* **1993**, *79*, 227−231.
(14) Avivi, S.; Mastati, Y.; Gedanken, A. *Chem. Mater.* **2000**, *12*, 1229−1233.
(15) Gurlo, A.; Ivanovskaya, M.; Barsan, N.; Schweizer-Berberich, M.; Weimar, U.; Göpel, W., Diequez, A. *Sens. Actuators B* **1997**, *44*, 327−333.

10.1021/cm031114n CCC: $25.00
Published on Web 10/11/2003

particles in the films deposited from the aged colloidal solution of indium hydroxide. However, the mechanism of the aggregation of $In(OH)_3$ nanoparticles is not very well understood, the details about the inner structure of these polycrystalline "aggregates" are missing, and their properties were not studied.

As known, the growth of the nanoparticles in the colloidal solution can occur by two primary mechanisms: Oswald ripening (coarsening or growth through dissolution) and growth involving aggregation.[16−18] It was recently shown that colloidal particles can also aggregate into large structures, and their aggregation does not always result in monocrystalline particles.[18−21] For example, in many cases the ordered aggregation of nuclei or small particles of a certain size (primary particles) is an important step in the mechanism of the formation of many monodispersed colloids.[22−24] As found, the latter consist of large particles, which are not necessarily single crystals and are usually made up of small subunits, even if they have well-defined geometric shape.[25−28] Recently, it was also shown that crystal growth by aggregation results in single crystals with iso-oriented mosaic textures.[29]

In this context we report the formation of well-shaped polycrystalline "blocks" made from nanosized units of indium oxide and give the direct evidence of their polycrystalline nature. One of the main findings of our work, which we believe is new, has been that the aggregation process changes the gas-sensing properties of indium oxide films.

In our previous works[18,19,29,30] it was shown that the thermal treatment of colloidal solution of indium hydroxide, peptized by nitric acid, leads to the formation of defect-rich cubic In_2O_{3-x} phase via three stages: (i) 100−120 °C, formation of the $In(OH)_3$ xerogel with structural OH^- and NO_3^- groups (shown by IR spectroscopy and by thermal analysis); (ii) 200−250 °C, decomposition and removal of OH^- and NO_3^- groups, crystallization of cubic In_2O_3 phase, stabilization of paramagnetic N-radicals in In_2O_3 structure (shown by electron paramagnetic resonance and thermal analysis); (iii) 400−500 °C, removal of N-radicals leads to the formation of defect-rich In_2O_{3-x} phase with $V_O^{\bullet}$, $In_i^{\bullet}$, and In_{In}' centers (Kröger-Vink notation). It was shown that these electronic centers play an important role in the detection of NO_2 and O_3.[19]

In the present study we have applied the sol−gel technique to prepare an $In(OH)_3$ colloidal dispersion and allowed it to age under controlled conditions to make possible the aggregation of the nanoparticles. Also, we studied, for the first time, the gas-sensing properties of well-shaped polycrystalline blocks of In_2O_3, made by aggregation of the nanoparticles in the colloidal solution.

Experimental Procedure

A. Preparation and Deposition. Indium nitrate (Aldrich, 99.9%), ammonia solution (Riedel-deHaën, 33%, weight), nitric acid (Aldrich, 70%), and bi-distilled water (Millipore Milli-Q plus RF, 18.2 MΩ) were used as starting materials for the preparation of the aqueous sol of indium hydroxide. Ammonia solution (1:10) was added dropwise to an aqueous indium nitrate solution (0.4 M) until pH = 8.5 (Hanna Instruments, p302). The so-formed precipitate was centrifugally separated (5000 rpm, 5 min), washed with bidistilled water, and peptized with nitric acid to obtain translucent, homogeneous, and stable sol. Keeping the as-prepared sol for 1 year leads to the sedimentation of the "white precipitate" from the sol (Figure 1). To study the structure and the properties of the samples containing the precipitate, the aged sol was carefully separated in two fractions: "aged colloidal solution" and "aged precipitate" (see Figure 1). The white precipitate was centrifugically (5000 rpm, 5 min) separated from the remaining aged colloidal solution and suspended in bidistilled water giving "aged suspension".

Thin and thick films were deposited from the as-prepared sol, and from the aged colloidal solution and the aged suspension on different substrates (sapphire, polished silicon, rough silicon, alumina, and alumina with interdigitated Pt electrodes) by using standard spin- and drop-coating techniques. To obtain thicker film, the coating procedure was repeated several times. Powders were obtained by calcination in air at 400 °C for 1 h (Carbolite tube furnace, CTF, static air) of the xerogels obtained by drying the as-prepared and the aged colloidal solution and the aged suspension in air at room temperature. This calcination temperature was chosen due to the complete phase transformation from $In(OH)_3$ into In_2O_3 and complete removal of N-radicals.[4,30]

The sensing layers were fabricated by drop-coating from the aged suspension and the aged colloidal solution on the alumina substrates with interdigitated Pt electrodes on the front side and heater on the backside. After deposition, the sensors were calcined at 400 °C in air for 1 h.

B. Characterization. Particle size distributions in solutions (e.g., in the as-prepared sol, in the aged colloidal solution, and in the aged suspension) were obtained by using photon correlation spectroscopy (Beckman Coulter N4 Plus, measurement at 90°) and sedimentation analysis (Shimadzu Centrifugal Particle Size Analyzer, SA-CP3, centrifugical mode, acceleration 120 rpm/min). The deposited films and powders were characterized by X-ray diffraction (XRD, a HZG-4a diffractometer, Cu Kα radiation, Ni monochromator), X-ray photoelectron spectroscopy (XPS, a VSW instrument, non-monochromatized Mg Kα radiation (1253.6 eV)), energy-dispersive X-ray spectroscopy (EDX Northern Tracor TN 5500 system with an accelerating voltage of 15 or 30 kV), transmission and scanning electron microscopy (TEM and SEM, Zeiss DSM 962, tungsten electrode, accelerating voltage of 15 or 30 kV), and high-resolution transmission electron microscopy (HRTEM). For HRTEM characterization, thin films deposited on silicon substrates (both on rough and mirror polished surfaces) were investigated by conventional bright-field and high-resolution imaging techniques and by selected area electron diffraction. The samples were prepared by mechanical polishing and ion thinning from the silicon side to reach the electron transparency. Alternatively, the In_2O_3 films were removed from the silicon substrate by a short exposure to hydro-fluoric acid vapors and a successive dipping into distilled water to separate

(16) Talapin, D. V.; Rogach, A. L.; Haase, M.; Weller, H. *J. Phys. Chem. B* **2001**, *105*, 12278.
(17) Hsu, J.-P.; Liu, B.-T. *Langmuir* **1999**, *15*, 5219−5226.
(18) Privman, V.; Goia, D. V.; Park, J.; Matijevic, E. *J. Colloid Interface Sci.* **1999**, *213*, 36−45.
(19) Penn, R. L.; Oskam, G.; Strathmann, T. J.; Searson, P. C.; Stone, A. T.; Veblen, D. R. *J. Phys. Chem. B* **2001**, *105*, 2177−2182.
(20) Banfield, J. F.; Welch, S. A.; Zhang, H.; Ebert, V.; Penn, R. L. *Science* **2000**, *289*, 751−754.
(21) Pileni, M. P. *Langmuir* **1997**, *13*, 3266−3276.
(22) Matijevic, E. *Chem. Mater.* **1993**, *5*, 412−426.
(23) Matijevic, E. *Langmuir* **1994**, *10*, 8−16.
(24) Ocana, M.; Serna, C. J.; Matijevic, E. *Colloid Polym. Sci.* **1995**, *273*, 681−684.
(25) Rogach, A. L.; Talapin, D. V.; Shevchenko, E. V.; Kornowski, A.; Haase, M.; Weller, H. *Adv. Funct. Mater.* **2002**, *12*, 653−664.
(26) Tian, Z. R.; Liu, J.; Voigt, J. A.; Mckenzie, B.; Xu, H. *Angew. Chem., Int. Ed.* **2003**, *42*, 414−417.
(27) Peng, X. *Adv. Mater.* **2003**, *15*, 459−463.
(28) Gou, L.; Murphy, C. J. *Nano Lett.* **2003**, *3*, 231−234.
(29) Cölfen, H.; Mann, S. *Angew. Chem., Int. Ed.* **2003**, *42*, 2350−2365.
(30) Ivanovskaya, M.; Bogdanov, P.; Gurlo, A.; Ivashkewich, L. *Inorg. Mater.* **1998**, *34*, 257−261.

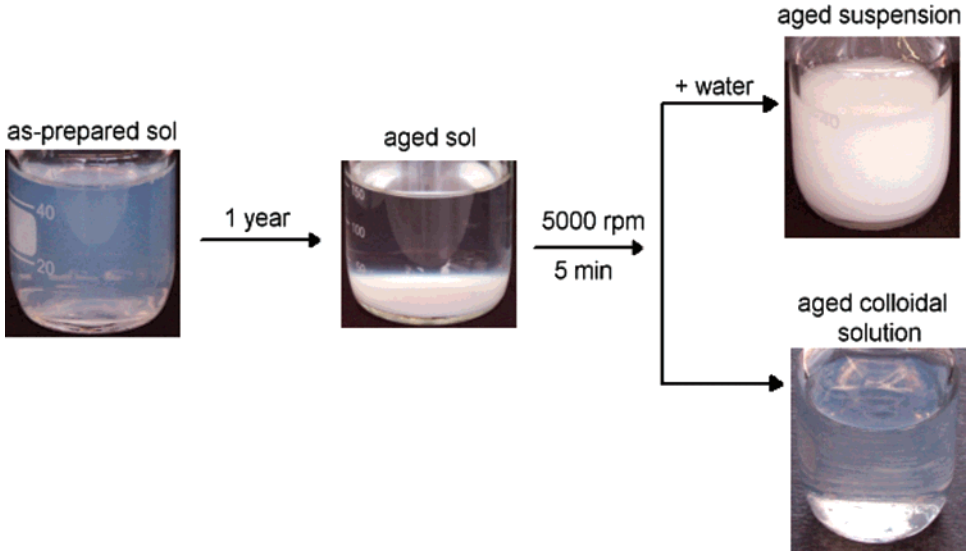

Figure 1. Scheme of the preparation and separation of the "aged sol" into the aged colloidal solution and the aged suspension fractions.

the film from the substrate; the floating film was collected on 400-mesh copper grids. Since there is no epitaxial orientation relationship between the substrate and the deposited films (as verified by a preliminary analysis performed on the samples prepared in the former way), the latter sample preparation allowed set-up of a more efficient method to prepare samples and to eliminate the contribution of the silicon substrate both from the image and particularly from the diffraction pattern (double diffraction effects). The comparison between the samples deposited on rough and mirror polished surfaces evidenced that the In_2O_3 films have the same morphological features, regardless of the substrate surface quality.

C. Characterization of the Gas-Sensing Properties by dc Electrical Tests. dc electrical measurements (sensor tests) have been performed to monitor the response to NO_2 and ozone in synthetic air with 50% relative humidity. The measurements were performed with a set of two identical sensors placed symmetrically in the Teflon-made test chamber and operated in the same conditions. The operating temperature of the sensors was adjusted between 200 and 350 °C. The sensor signal is given in the following as the resistance ratio R_{gas}/R_{air} for NO_2 and ozone and as R_{air}/R_{gas} for CO and ethanol, where R_{gas} and R_{air} denote the sensors' resistances in the presence and in the absence of NO_2, O_3, CO, and ethanol, respectively. A computer-driven gas-mixing system provided the analyte gas. A typical gas mixing bench consists of a combination of computer-controlled mass flow controllers and computer-controlled valves (for the details of the experimental setup, see ref 31). The sensors were exposed to NO_2 (200−900 ppb), O_3 (30−900 ppb), CO (250 ppm), and ethanol (250 ppm) in synthetic air at 50% RH at 300 °C. The humidity was adjusted by bubbling synthetic air through a column of water and subsequently mixing it with dry air in a gas blender. In a typical measurement, 20 or 60 min of analyte exposure was alternated with 20 or 60 min of carrier gas exposures. Defined concentrations of NO_2, CO, ethanol, and O_3 were obtained in the PC-controlled gas-mixing bench by mixing certified NO_2, CO, or ethanol test gas (Praxair) and ozone; the latter was produced by using an Anseros ozone test system SIM 6000 with an integrated ozone generator and MP UV ozone analyzer. Incoming NO_2 and O_3 concentrations were controlled by ML 9841B NO_x Chemiluminescence and Environics Series 300 computerized UV ozone analyzers, respectively.[32]

(31) Kappler, J.; Tomescu, A.; Barsan, N.; Weimar, U. *Thin Solid Films* **2001**, *391*, 186−191.

(32) Gurlo, A.; Barsan, N.; Weimar, U. XIV Eur. Conf. on Solid State Transducers "Eurosensors XVI" 2002, Prague, Czech Republic, WP18.

Table 1. Mean Particle Size Determined in the Solutions by Photon Correlation Spectroscopy (PCS) and Centrifugical Analysis and in the Powders Calcined at 400 °C

	sol		powder, calcined at 400 °C	
sample	PCS, 90°	sedimentation	TEM, powder	XRD, powder
as-prepared sol	13 nm	<20 nm	5 nm	8 nm
aged colloidal solution	13 nm	<20 nm	6 nm	10 nm
aged suspension	>1 μm	1.19 μm	6 nm	11 nm

Results and Discussion

As-Prepared Sol. A typical size distribution of the particles in the as-prepared sol is shown in Figure 1. The $In(OH)_3$ particles have mainly the same size (≈13 nm) and possess a spherical shape. The shape of the particles remains after the calcinations, as shown by transmission electron microscopy. Up to an annealing temperature of 400 °C, there were no significant changes in the particle size as well as in the size distribution. Thin films and powders calcined at 400 °C are composed of nearly spherical particles with narrow size distribution and an average diameter ≈5−8 nm (Table 1, Figure 2). The X-ray diffraction patterns (not shown here) show that both the films and powders are composed of cubic In_2O_3 (JCPDS Card 060416). The electron diffraction patterns additionally show the possible presence of hexagonal In_2O_3 ($d \approx 2.42$ Å, JCPDS card 0220336).

Aged Sol. As mentioned above, keeping the as-prepared sol for 1 year leads to the sedimentation of the white precipitate. Careful separation of the aged sol into two fractions, aged suspension and aged colloidal solution, is described in the Experimental Procedure section and is shown schematically in Figure 1. Analysis of the particle size in the aged colloidal solution shows that there are no significant changes both in the mean particle diameter (≈13 nm) and in the size distribution in comparison with that of the as-prepared sol (Figure 3A and B). This shows that the size of the primary particles in the colloidal solution has not changed and it has excluded the growth of the particles by Oswald

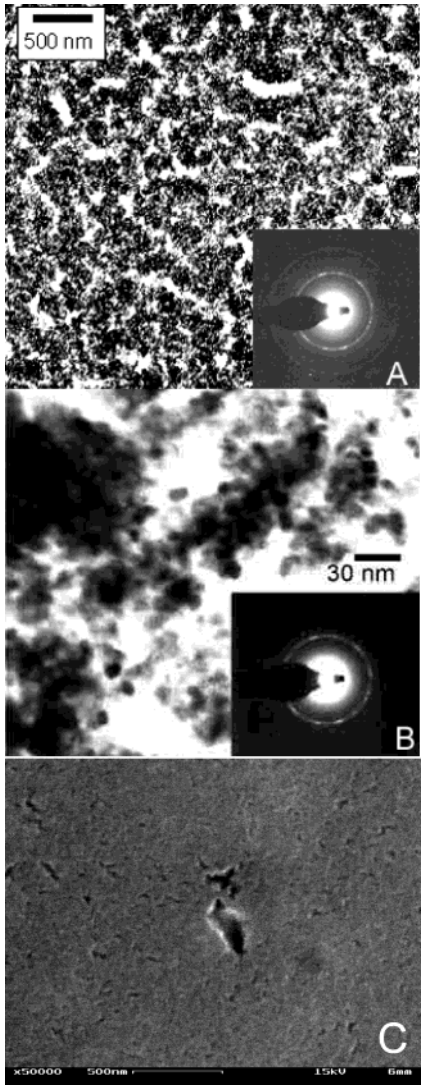

Figure 2. Typical transmission (A, B) and scanning (C) electron microscopy pictures of the film (A, C) and powder (B), deposited from the as-prepared sol and calcined at 400 °C in air for 1 h. The insets show the electron diffraction patterns.

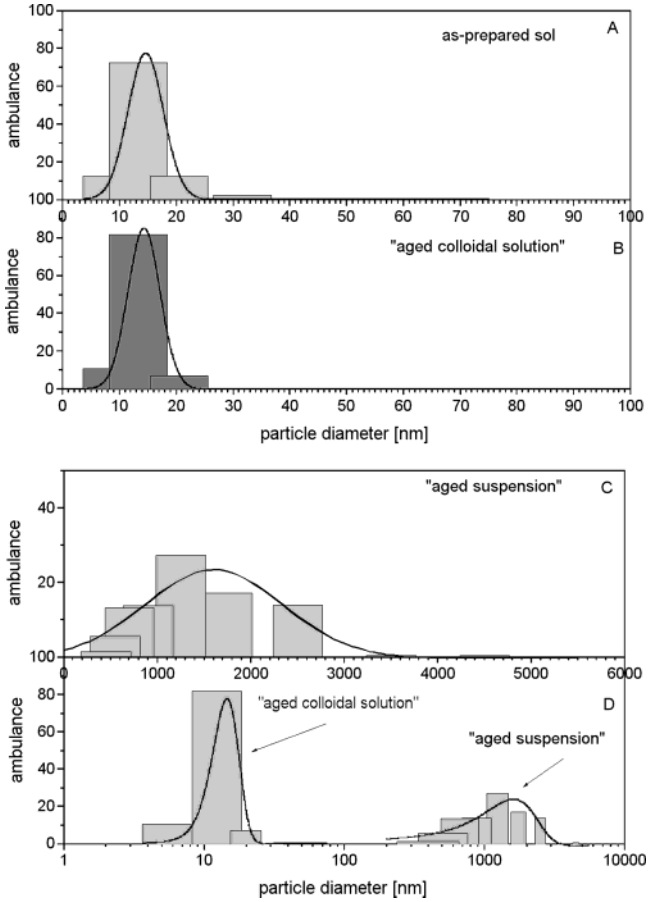

Figure 3. Size distribution in the as-prepared sol (A, photon correlation spectroscopy analysis), in the aged colloidal solution (B, photon correlation spectroscopy analysis), and in the aged suspension (C, sedimentation analysis). (For better comparison, the distributions for the aged colloidal solution and for the aged suspension are present on the same scale (D)). As an optical guideline, the corresponding fitted data assuming a Gaussian distribution are shown as lines in this diagram.

ripening. On the other hand, the mean particle diameter in the aged suspension is detected to be ≈1.19 μm (Figure 3C,D). SEM picture of the film deposited from the aged suspension and dried in the air at room temperature shows that the film is composed of well-shaped "blocks" and "bricks" (Figure 4). The shape of the blocks remains after the calcinations at 400 °C and the phase transformation from $In(OH)_3$ into In_2O_3 (Figure 5). The films and powders calcined at this temperature are composed of the rectangular blocks with a dimension between several hundreds of nanometers and several micrometers; the blocks are composed of aggregated tiny subunits with an average diameter of ≈12 nm. XRD patterns show (not shown here) that the samples are polycrystalline and composed of cubic In_2O_3. The crystallite size of the nanosized particles, as calculated from the Scherrer equation, is ≈11 nm. The Electron diffraction patterns additionally show the possible presence of hexagonal In_2O_3 ($d \approx 2.42$ Å, JCPDS card 0220336) in the film.

To obtain more detailed information about the inner structure of the blocks, In_2O_3 films composed of blocks are studied by HRTEM. As shown in the low-magnification bright-field image reported in the Figure 6, the morphology of the films is characterized by parallelepiped-shape grains, whose minor size and major size are respectively <100 nm and <1 μm. The selected area diffraction pattern shows that these structures have a polycrystalline-textured feature; from the interpretation of the diffraction pattern, it turns out that the In_2O_3 grains are a mixture of cubic (JCPDS card 060416) and hexagonal (JCPDS card 0220336) phases. The experimental interplanar spacings obtained from the diffraction pattern are reported in the table below and compared with the theoretical values of both the In_2O_3 cubic and hexagonal phases (Table 2). As proved by higher magnification bright field images, each parallelepiped exhibits Moirè fringes of different spacing and orientation: since Moirè's patterns come from the overlapping of misoriented crystals or crystals having different crystallographic structure, it turns out that each parallelepiped has a polycrystallline nature. This is also confirmed by the feature of the lattice fringes in the high-resolution images.

As known, under normal conditions In_2O_3 crystallizes in cubic bixbyite-type structure (cubic-In_2O_3, space group *Ia*3, the cell contains 16 units).[33] Corundum-type

(33) Marezio, M. *Acta Crystallogr.* **1966**, *20*, 723−728.

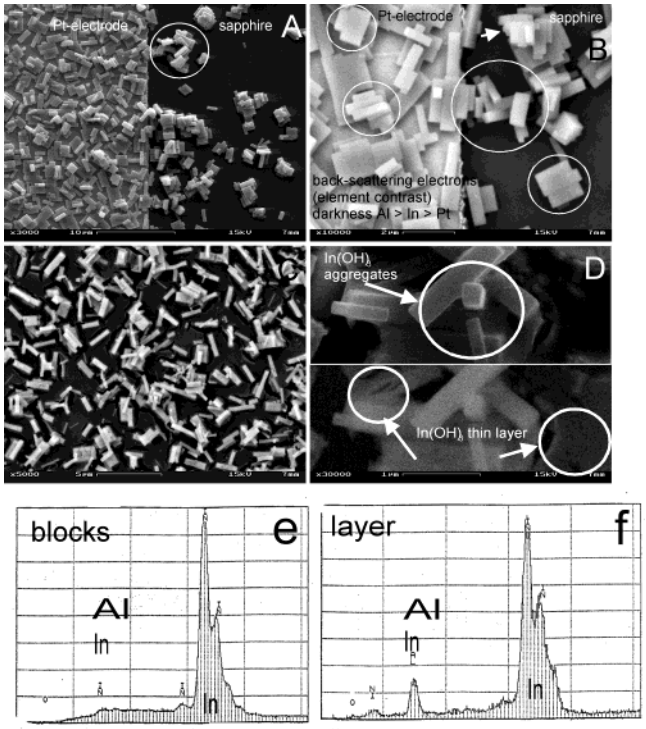

Figure 4. Scanning electron microscopy pictures (A−D) of the films, deposited from the aged suspension on a sapphire substrate with Pt electrodes and dried in air at room temperature; (A) secondary electron mode, (B) backscattering electron mode. Energy-dispersive X-ray spectroscopy (EDX) spectra (part) from the aggregates (blocks, E) and thin film (F).

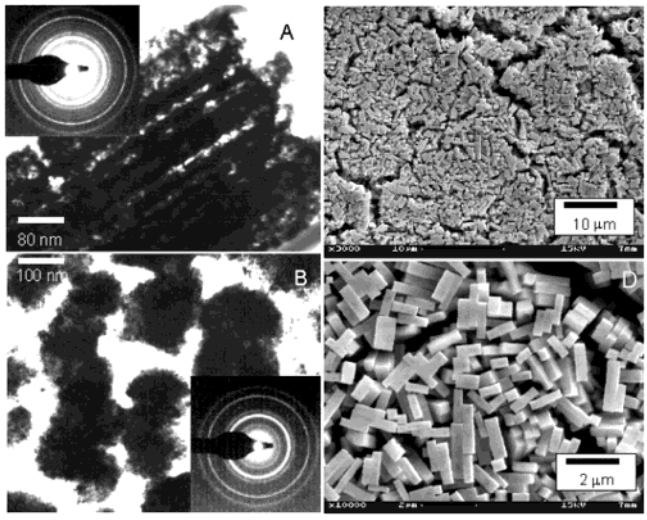

Figure 5. Transmission (A, B) and scanning (C, D) electron microscopy pictures of the films (A, C, D) and powder (B), deposited from the aged sol and calcined at 400 °C. The insets show the electron diffraction patterns.

indium(III) oxide (hexagonal-In_2O_3, space group $R\bar{3}c$, the cell contains 6 formula units) is known to be the high-pressure modification of In_2O_3.[34,35] The cubic to hexagonal phase transition under ambient conditions is supposed to be favored when a foreign atom M (Fe^{3+}, Sn^{4+}) with a smaller ionic radius than indium is

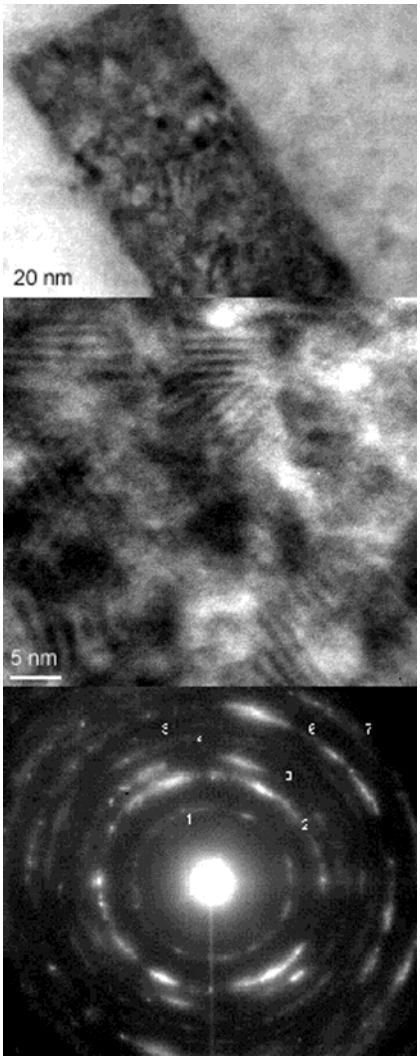

Figure 6. Transmission electron microscopy (A, B) and selected area electron diffraction patterns (C) pictures of the films, deposited from the aged suspension and calcined at 400 °C in air.

Table 2. Experimental and Literature Interplanar Spacings Obtained from the Diffraction Pattern (Selected Area Electron Diffraction) for the In_2O_3 Film, Deposited from the "Aged Suspension" and Calcined at 400 °C in Air

	literature, cubic In_2O_3		literature, hexagonal In_2O_3	
experimental	JCPDS card 060416		JCPDS card 0220336	
d [Å]	d [Å]	(hkl)	d [Å]	(hkl)
$d_1 = 3.9$			3.97	(012)
$d_2 = 2.88$	2.92	(222)	2.88	(104)
$d_3 = 2.48$	2.53	(400)		
$d_4 = 2.30$			2.38	(113)
$d_5 = 2.06$	2.06	(422)		
$d_6 = 1.95$			1.98	(024)
$d_7 = 1.74$	1.788	(440)	1.81	(116)

inserted into the cubic indium oxide network.[36−40] The formation of hexagonal In_2O_3 under ambient conditions without any doping is quite unusual and not understood

(34) Prewitt, C. T.; Shannon, R. D.; Rogers, D. B.; Sleight, A. W. *Inorg. Chem.* **1969**, *8*, 1985−1993.
(35) Christensen, A. N.; Broch, N. C.; Heidenstam, O.; Nilsson, A. *Acta Chem. Scand.* **1967**, *21*, 1046−1056.
(36) Frank, G.; Olazcuaga, R.; Rabenau, A. *Inorg. Chem.* **1977**, *16*, 1251−1253.
(37) Kim, B.-C.; Kim, J.-Y.; Chang, S.-H. *Mater. Res. Soc. Symp. Proc.* **2000**, *581*, 27−32.

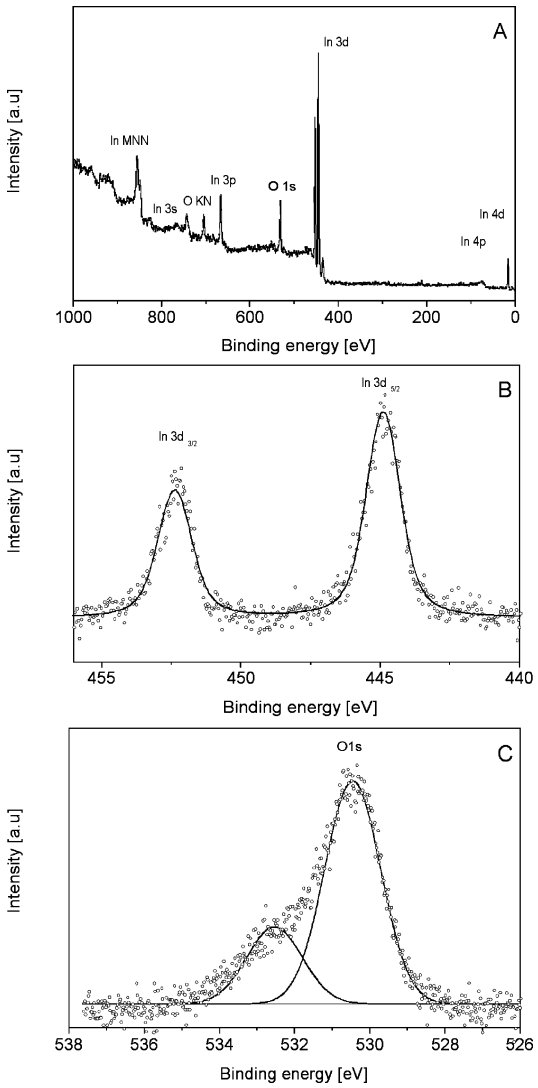

Figure 7. XPS survey (A), In 3d (B) and O 1s (C) core level XPS spectra of the film deposited from the aged suspension and calcined at 400 °C in air.

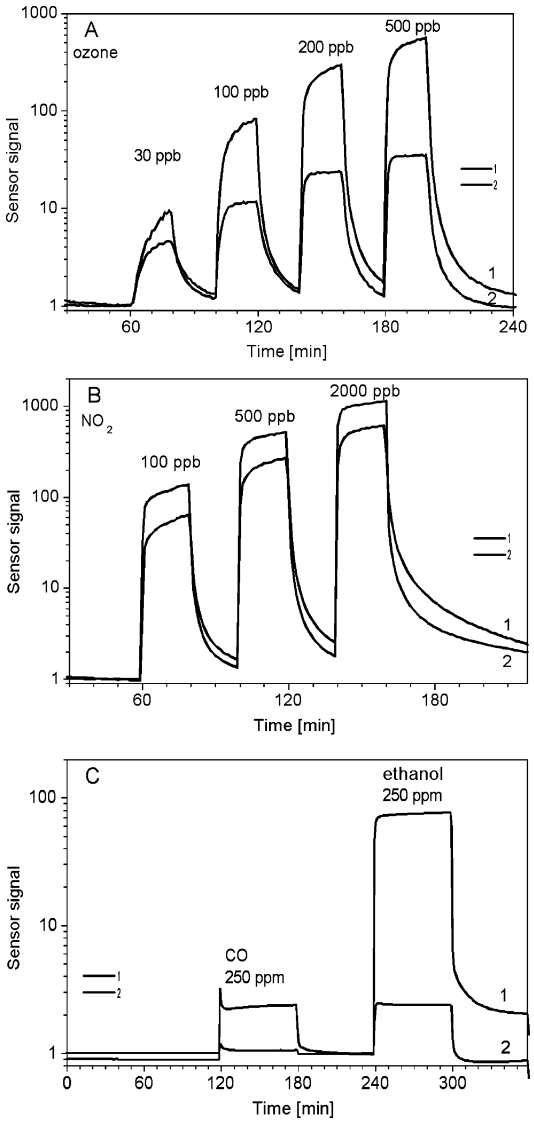

Figure 8. Sensor signal of In_2O_3 sensors at 300 °C in 50% r.h. air to ozone (A), nitrogen dioxide (B), and CO and ethanol vapor (C) as the concentration is varied from 30 to 500 ppb (ozone), from 200 to 2000 ppb (nitrogen dioxide), and 250 ppm (CO and ethanol); 1, film deposited from the aged suspension, and 2, film, deposited from aged colloidal solution.

until now. We have to mention that there is no evidence that the formation of the hexagonal phase is related to the aggregation process. Hexagonal In_2O_3 was already observed[30] in the sol−gel-prepared In_2O_3 films, which did not show any unusual aggregation behavior. Moreover, the hexagonal phase was presumably detected in the films deposited both from the as-prepared sol and from the aged colloidal solution. However, we have to mention that the given assignment is quite questionable due to the fairly low crystallinity of the samples and resulting broadening of corresponding ED patterns.

A typical XPS spectrum of the film deposited from the aged suspension and calcined at 400 °C is shown in Figure 7. The In_2O_3 spectrum exhibits the characteristic spin−orbit split $3d_{5/2}$ and $3d_{3/2}$ signals and a O 1s peak (Figure 7b). The O 1s XPS signals (Figure 7c) of the sample could be deconvoluted into two components—two Gauss−Lorenz peaks with the same fwhm of 1.7 eV for both the peaks. The observed O 1s peak at 530.7 eV can be assigned to the lattice oxygen in crystalline In_2O_3 and the O 1s peak at 532.5 eV to adsorbed OH groups or to adsorbed oxygen species ($O_m^{\delta-}$). The results of the XPS investigations are very similar to the reported ones on the In_2O_3 films deposited from the as-prepared sol.[18] It means that the main composition of the surface did not change due to the aggregation of the nanoparticles.

Gas-Sensing Properties. Exposure of oxidizing gases (NO_2 and ozone) increases the resistance of the sensors (Figure 8A and B) and exposure of reducing gases (ethanol and CO) decreases the resistance of the sensors (Figure 8C). This behavior is typical for the indium oxide as an n-type semiconductor. The most interesting findings is that the gas-sensing properties of the layers deposited from the aged colloidal solution and from the aged suspension are completely different. The former one is almost insensitive to CO and ethanol in air, and the latter one shows good response to CO and ethanol (Figure 8E). However, the sensors show

(38) Parent, Ph.; Dexpert, H.; Tourillon, G.; Grimal, J.-M. *J. Electrochem. Soc.* **1992**, *139*, 276−281.
(39) Malik, A.; Nunes, R.; Martins, R. *Mater. Res. Soc. Symp. Proc.* **1998**, *481*, 599−604.
(40) Gurlo, A.; Ivanovskaya, M.; Barsan, N.; Weimar, U. *Inorg. Chem. Commun.* **2003**, *6*, 569−573.

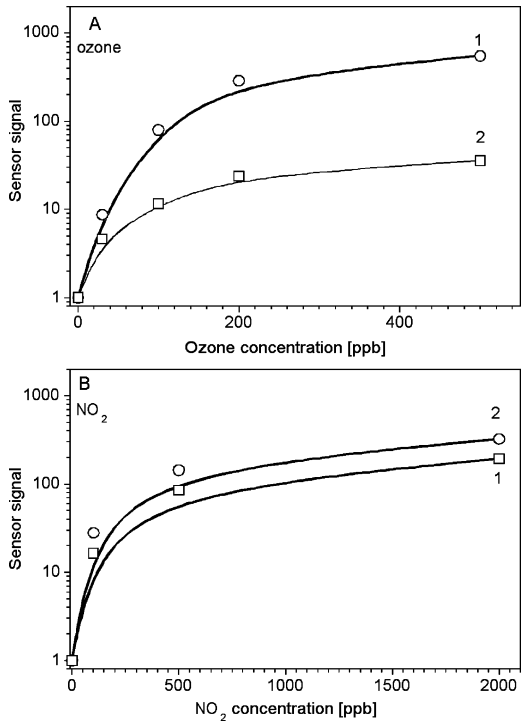

Figure 9. Concentration dependence of the sensor signal to ozone (A) and to nitrogen dioxide (B); 1, film deposited from the aged suspension, and 2, film, deposited from aged colloidal solution.

much higher signals to oxidizing gases than to reducing gases. It is noteworthy that the exposure of nitrogen dioxide or ozone even at the low-concentration levels (less than 500 ppb) leads to the drastic increase in the sensor resistance (more than 500 times).

Generally, an increase of sensor resistance can be associated with a chemisorption process and explain in terms of an electron transfer from the semiconductor (indium oxide) to adsorbed surface species. Until now, the nature and origin of the surface species in the case of the detection of ozone and nitrogen dioxide is under discussion (for details, please see refs 19 and 32). Shortly, one extreme case is the detection of NO_2 and ozone through the dissociative adsorption ("consumption") of NO_2 and ozone molecules and the formation of adsorbed oxygen species on the oxide surface. The other extreme case is the detection of NO_2 and ozone through the adsorption−desorption of NO_2 and ozone molecules. The adsorption of NO_2 can lead to the formation of uni- and bidentate surface nitrate ($[O_{surf}-NO_2]^-$) or nitrito species ($[M_{surf}-NO_2]^{n+}$). The decomposition of surface species can lead to the desorption of NO or N_2 in the gas phase. The dissociative adsorption of ozone can lead to the formation of different surface oxygen species (for example, O_3^-, O_2^-, and O^-). One should keep in mind that the mechanism of NO_2 and ozone interaction can depend on the operating temperature of the sensors and on the gas concentration range. Usually, it is assumed that metal oxide sensors work through adsorption−desorption of the target gas at low temperatures and through decomposition at high temperatures.

Figure 9 clearly shows the difference between the layers deposited from the aged suspension and the aged colloidal solution. In_2O_3 layers deposited from aged suspension and composed of well-shaped blocks are much more sensitive to low concentrations (30−500 ppb) of ozone than to comparable concentrations of nitrogen dioxide in air. On the other hand, In_2O_3 films deposited from the aged colloidal solution show almost the same signal to the comparable concentrations of nitrogen dioxide and ozone (Figure 9A,B). The difference in the gas-sensing properties between the films deposited from the aged suspension and from the aged colloidal solution cannot be caused only by the difference in the film thickness because it was not observed for the thin and thick films deposited from the as-prepared sol.[32] Although a recently published paper dealing with the gas-sensing properties of different indium oxide phases[41] showed that the sensitivity to reducing gases (ethanol vapor) of thick film semiconducting sensors based on hexagonal In_2O_3 was higher in comparison with the one based on cubic In_2O_3, on the basis of the results presented here, the different electrical behavior cannot be ascribed to the different crystalline phases of the films, too. The reason this happens here is to be understood.

Conclusions

In summary, we demonstrate that the aging-induced aggregation of precursor nanoparticles in the colloidal solution of indium hydroxide leads to the formation of well-shaped polycrystalline particles and changes the gas-sensing properties of the prepared indium oxide films. A tuning of the sensors sensitivity toward ozone or nitrogen dioxide is possible by suitable selection of the materials resulting from the aging of the same starting solution.

Acknowledgment. This work was performed in the frame of GASMOH, ICA2-CT-2000-10041 project.

CM031114N

(41) Kim, B.-C.; Kim, J.-Y.; Lee, D.-D., Lim, J.-O.; Huh, J.-S. *Sens. Actuators B* **2003**, *89*, 180−186.